Sensitivity enhancement of grating interferometer based two-dimensional sensor arrays using two-wavelength readout

Onur Ferhanoglu and Hakan Urey*

Department of Electrical Engineering, Optical Microsystems Laboratory, Koç University, Sarıyer, Istanbul 34450, Turkey

*Corresponding author: hurey@ku.edu.tr

Received 8 December 2010; revised 5 May 2011; accepted 10 May 2011; posted 13 May 2011 (Doc. ID 139104); published 29 June 2011

Diffraction gratings integrated with microelectromechanical systems (MEMS) sensors offer displacement measurements with subnanometer sensitivity. However, the sensitivity of the interferometric readout may drop significantly based on the gap between the grating and the reference surface. A two-wavelength ($2-\lambda$) readout method was previously tested using a single MEMS sensor for illustrating increased displacement measurement capability. This work demonstrates sensitivity enhancement on a sensor array with large scale parallelization ($\sim 20,000$ sensors). The statistical representation, which is developed to model sensitivity enhancement within a grating based sensor array, is supported by experimental results using a thermal sensor array. In the experiments, two lasers at different wavelengths (633 and 650 nm) illuminate the thermal sensor array from the backside, time-sequentially. The diffracted first order light from the array is imaged onto a single CCD camera. The target scene is reconstructed by observing the change in the first diffracted order diffraction intensity for both wavelengths. Merging of the data from two measurements with two lasers was performed by taking the larger of the two CCD measurements with respect to the reference image for each sensor. ~30% increase in the average sensitivity was demonstrated for a 160 × 120 pixel IR sensor array. Proposed architecture is also applicable to a variety of sensing applications, such as parallel biosensing and atomic force microscopy, for improved displacement measurements and enhanced sensitivity.

OCIS codes: 050.1950, 120.3180, 120.2830.

1. Introduction

Diffracting gratings embedded under microelectromechanical systems (MEMS) sensors provide subnanometer displacement measurements for various sensing and imaging applications such as atomic force microscopy [1,2], MEMS based Fourier transform IR spectrometers [3,4], biomolecular force spectroscopy sensors [5], resonant mass biosensors [6,7] and thermal imaging [8,9]. A displacement resolution as low as $3\,\mathrm{fm}\cdot\mathrm{Hz}^{-1/2}$ was demonstrated by state of the art membrane based force measurement sensors incorporating diffraction grating readout [5].

Despite its ultrahigh displacement sensitivity, interferometer based readouts are limited to an unambiguous range of $\lambda/4$ for a single, narrowband illumination source. Furthermore, the sensitivity may be degraded significantly based on the sensor position. For active sensors where the gap between the sensor and diffraction grating can be controlled, the gap is typically tuned to the maximum sensitivity given by the highest slope of the intensity versus gap curve. When the sensor is tuned for maximum sensitivity, a displacement of $\lambda/8$ brings the sensor sensitivity essentially to zero. Recently, an integrated dual-grating method has been proposed [10], where two gratings with $\lambda/8$ height difference that results in a 90° phase shift to the incoming light are placed underneath a membrane sensor. The quadrature

0003-6935/11/193289-07$15.00/0

signal acquired using phase-shifted double grating, results in constant sensitivity that is equal to the sensitivity achieved at the maximum sensitivity point using a single grating. Another method for achieving constant, high sensitivity and extended range readout was demonstrated through active control of a micromachined scanning grating interferometer. The sensor was electrostatically controlled using a modified recurrent calibration based path stabilization algorithm [11] to remain at the maximum sensitivity point.

The aforementioned methods are beneficial for either a dual-grating based sensor that can afford a significant amount of space for its reference reflector or an active sensor whose gap can be controlled. Integrating multiple sources into the readout is a robust solution especially for passive sensor arrays, which enhances both the range and the sensitivity of the displacement measurement. $2-\lambda$ interferometry was first implemented starting in the early 1970s [12,13]. The $2-\lambda$ readout for diffraction grating interferometers as a method for maintaining the sensitivity for a large range of displacements were previously demonstrated [14,15]. The most important advantages of the $2-\lambda$ readout of grating based sensor arrays can be summarized below.

1. No change in the sensor structure: an additional laser source can be placed in the optical train without difficulty.
2. No electrical interconnects to the sensor: the $2-\lambda$ readout method requires no active tuning of the sensor that makes it more suitable for passive sensor applications such as the thermal imaging sensor arrays [8,9].
3. Extended range: using the $2-\lambda$ readout method, the unambiguous displacement detection range is increased from quarter wavelength $\lambda_1/4$ up to $(\lambda_1 \cdot \lambda_2)/4|\lambda_1-\lambda_2|$, where λ_1 and λ_2 are the readout wavelengths. For $\lambda_1 = 650\,\text{nm}$ and $\lambda_2 = 633\,\text{nm}$, this implies an enhancement of the range from 160 nm up to $6\,\mu\text{m}$. This advantage was previously demonstrated using a dynamic diffraction grating based Fourier transform spectrometer [14].
4. Enhanced sensitivity: the $2-\lambda$ readout method provides displacement measurement up to the $\sim 1\,\mu\text{m}$ range with $>60\%$ maximum sensitivity and the $\sim 1.7\,\mu\text{m}$ range with $>50\%$ maximum sensitivity using the above wavelengths. Corresponding ranges for the single wavelength readout case ($\lambda = 633\,\text{nm}$) are only 95 and 105 nm, respectively.

This paper presents the basic $2-\lambda$ sensor readout principle, defines the sensitivity of the $2-\lambda$ readout method, and extends the analytical modeling to a two-dimensional (2D) array of sensors considering the statistical variations of various nonuniformities inherent in the sensor. Experimental demonstration of the sensitivity improvement is performed on a 2D grating based thermal imaging sensor array with 20, 000 sensors.

2. Two-Wavelength Grating Interferometry

Figure 1(a) illustrates a diffracting grating based sensor. The sensor is fabricated on a transparent substrate and consists of an embedded fixed grating placed underneath the sensor and a reflector that is placed on top of the sensor. The illumination is performed from the bottom side. Fixed grating and the reflector form an interferometer where the movement of the sensor modulates the optical path difference and the resultant diffraction order intensities. Well known formulas for the zeroth and odd diffracted order light can be expressed as

$$I_0\,\alpha\left(\cos\left(\frac{2\pi g}{\lambda}\right)\right)^2, \tag{1}$$

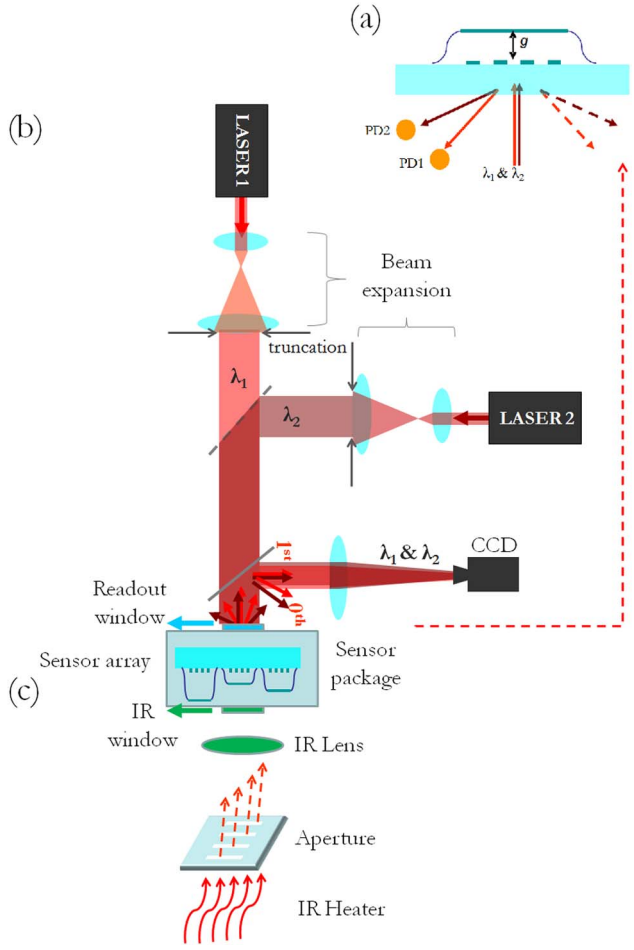

Fig. 1. (Color online) (a) Diffraction grating based MEMS sensor on a transparent substrate that is illuminated with two lasers with wavelengths λ_1 and λ_2 (b) Proposed method using two-wavelength illumination where the sensor array, with gap variation, is illuminated by two sources, one at a time. The diffracted first order light is imaged onto an array of photodetectors, i.e., a CCD camera. (c) Details of the thermal imaging experiment where the blackbody radiation emitted from an IR heater that is covered with an aperture is imaged onto the thermomechanical sensor array.

$$I_{\text{odd}} \alpha \left(\sin\left(\frac{2\pi g}{\lambda}\right)\right)^2, \tag{2}$$

where g is the gap between the sensor and the fixed grating and λ is the wavelength of illumination. Since the intensity variation of all orders is periodic with respect to g, the range of the interferometric readout is bounded to an unambiguous range of $\lambda/4$. Furthermore, the sensitivity, defined as the rate of change of intensity with a gap, can severely diminish near the peaks and the dips of the sinusoidal intensity curve. Note that the highest absolute sensitivity is achieved where $g = \lambda/8 + k\cdot\lambda/4$ and the lowest (zero) sensitivity is achieved where $g = k\cdot\lambda/4$ for any positive integer k.

Figure 1(b) illustrates a setup suitable for the sensor array readout by monitoring first diffraction orders with a single CCD camera. The 2D sensor array is uniformly illuminated in one shot, by expanding and truncating two lasers with wavelengths λ_1 and λ_2 time-sequentially. Alternatively, the readout can be accomplished by monitoring each source with a different camera simultaneously, in the expense of higher cost and larger space. The normalized sensitivity for either one of the wavelengths and the combined sensitivity of the $2-\lambda$ readout system for the first diffracted order can be defined as [14]

$$S(\lambda,g) = |dI(\lambda,g)/dg| = \left|\frac{2\pi}{\lambda}\sin\left(\frac{4\pi}{\lambda}g\right)\right|, \tag{3}$$

$$S_{2\lambda}(\lambda_1,\lambda_2,g) = \left[\frac{\min[\lambda_1,\lambda_2]}{2\pi}\right]\max[S(\lambda_1,g),S(\lambda_2,g)], \tag{4}$$

where $S_{2\lambda}$ is the sensitivity of a sensor under two wave illumination and takes on the higher sensitivity value of the two sensitivity measurements performed using λ_1 and λ_2 separately. λ_1 and λ_2 sources are considered to be adjusted to equal intensity levels; therefore, $S_{2\lambda}$ is normalized with respect to the minimum wavelength, as the lower wavelength results in higher sensitivity for a fixed intensity level. For similar wavelength sources having equal intensity, the sensitivity difference is negligible.

A calibration routine involving a reference frame and two consecutive frames captured with λ_1 and λ_2 at a different gap are necessary to identify which wavelength result in higher sensitivity for each pixel. This calibration may also be used for correcting spatial variations of the illumination beams, which loosens the requirements of having equal intensity sources or perfect beam homogenization. Results can then be stored in a look-up-table. For the thermal sensor array used in the experiments, the gap can be varied by changing the sensor die temperature via its controller or by imaging a uniform temperature object at a near ambient temperature. Figure 1(c) illustrates the thermal imaging experimental setup, which is described in detail at the Experimental Results Section. This part of the setup is subject to modification for other applications.

Selection of λ_1 and λ_2 plays a critical role on the amount of measurement range and the $S_{2\lambda}$ sensitivity. The maximum unambiguous detection range for the $2-\lambda$ system, also called the synthetic wavelength λ_S, is defined as [13]

$$\lambda_S = \frac{\lambda_1\cdot\lambda_2}{|\lambda_1-\lambda_2|}. \tag{5}$$

The unambiguous detection range increases from $\lambda/4$ for one laser readout to $\lambda_S/4$ for the $2-\lambda$ readout. The highest overall sensitivity $S_{2\lambda}$ is achieved when $g = \lambda_S/8$ [14,15]. Therefore, λ_1 and λ_2 should be selected such that $\lambda_S = 8g$.

There are more than one choice of wavelength pairs that could satisfy a specified "g". Lower wavelengths result in higher slopes according to Eq. (3); however, they are not favorable due to the monitor detector constraints. Majority of the silicon detectors exhibit peak sensitivity at $\lambda > 500\,\text{nm}$ [16]. Although silicon detectors exhibit very high sensitivities at $\lambda > 750\,\text{nm}$, higher wavelengths are undesirable both due to the decrease of the readout sensitivity $S(\lambda,g)$ and decrease of the visibility for the human eye, which makes alignment in a benchtop system more tedious. Based on availability, cost and all above constraints, we preferred to use red lasers ($600\,\text{nm} < \lambda < 700\,\text{nm}$) for theoretical analysis and experiments.

A wide range of red laser diodes emitting at different wavelengths are available in the market ($\lambda = 635$, 637, 639, 640, 642, 650, 658, 660, 670, 685, 690, 700 nm) from which illumination sources can be selected [16]. Based on Eq. (5) and available laser diode wavelengths, it is possible to achieve an optimal sensitivity gap from 1 up to 25 μm. Intermediate gap values can be addressed exploiting different wavelength combinations as well, without the need for a tunable, high cost laser light source.

Laser stability and bandwidth ($\Delta\lambda$) are other crucial elements that determine the amount of displacement enhancement for readout using two wavelengths. Laser bandwidth determines the coherence length ($\lambda^2/\Delta\lambda$) of the interferogram that sets a limit for the maximum detectable displacement. Therefore, the coherence length of both sources should be $>\lambda_S/4$. Furthermore, the stability tolerance for a given detection range can be as severe as $\lambda/1000$ [17]. Battery operated, low cost laser diode control units are available in the market, which can precisely control the feed current and temperature in order to satisfy the stability tolerances.

3. Analytical Modeling

Analytical modeling is established considering the thermal imaging sensor that is used in the experiments. The model addresses readout sensitivity with respect to statistical gap variations and is adaptable

to any type of grating based sensor array. The mean gap of thermal imaging sensor arrays operating in the 8–14 μm long wave IR wavelength range is typically around 2.25 μm [9]. The two wavelengths considered for the readout are $\lambda_1 = 650$ nm and $\lambda_2 = 633$ nm, respectively. The sensitivity around the mean gap (g_0), assuming the same gap value for λ_1 and λ_2 measurements, is calculated using Eq. (3) and can be observed in Fig. 2. At $g_0 = 2.25\,\mu$m, the normalized sensitivity (normalization is performed with respect to the maximum sensitivity) is ~0.5 for both wavelengths. The overall sensitivity increases with temperature change, as the arrows suggest: a decrease of gap causes an increase in the sensitivity of the λ_1 readout and an increase in the gap causes an increase in the sensitivity of the λ_2 readout setting a lower limit of 0.5 for the sensitivity [14,15].

For statistical analysis, the gap of each sensor within the array is modeled as random variable, such that

$$g = N(g_0, \sigma), \tag{6}$$

where N stands for a normal distribution (Gaussian random variable). As previously mentioned, $g_0 = 2.25\,\mu$m and three different standard deviation values were investigated: $\sigma = 10, 15, 20$ nm. Two approaches are followed for calculating the sensitivity of 2000 pixels in the array that provides large enough sample space for the numerical simulations.

i. The synchronous approach assumes that the sensor gap remains constant in between λ_1 and λ_2 measurements. This approach is valid where sensor displacements within one frame can be neglected, or two monitoring cameras are used to capture different sources simultaneously. Therefore, the gap distribution of the sensor array for both measurements are equal such that $g = g_1 = g_2 = N(g_0, \sigma)$. The overall sensitivity is then calculated using Eq. (4).

ii. The asynchronous approach assumes the gap changes between two measurements performed with λ_1 and λ_2. For a thermal imaging sensor array [9], this approach accounts for any temperature or position change of the target between measurements. Assuming a small and independent change between measurements that slightly alters individual sensor gaps without significantly changing overall gap statistics (such as a movement or shift of the target between measurements), the gap distributions g_1 and g_2 during λ_1 and λ_2 measurements are taken as independent random variables with the same statistical properties, such that $g_1 = N(g_0, \sigma)$ and $g_2 = N(g_0, \sigma)$. (The overall sensitivity is calculated based on Eq. (4) using g_1 and g_2 on the right side of the equation instead of g).

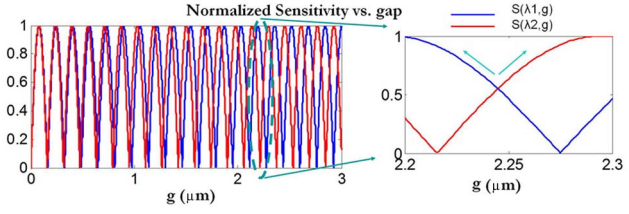

Fig. 2. (Color online) Sensitivities: $S(\lambda_1, g)$ and $S(\lambda_2, g)$ with respect to the gap change. Any displacement around the mean gap: $g_0 = 2.25\,\mu$m causes an increase in the combined sensitivity.

Figure 3 illustrates expected sensitivity histograms for λ_1 and λ_2 measurements based on both approaches (same and different sets of gaps for λ_1 and λ_2 measurements) for $\sigma = 10, 15, 20$ nm. A sensitivity enhancement of 20%–40% is observed on the average sensitivity. The sensitivity enhancement with the $2-\lambda$ readout is higher at higher σ values, where the gap variation within the sensor array is less uniform, as expected. Furthermore, the sensitivity histograms are more spread out for higher σ values. The $2-\lambda$ readout method is beneficial where there is significant gap variation among the array elements (large σ), and it converges to the sensitivity of a single wavelength readout if the gap is constant for all array elements.

The combined sensitivity histograms using the synchronous approach exhibits a minimum sensitivity limit as previously described and illustrated in Fig. 2. On the other hand, the combined histograms calculated with the asynchronous approach are smooth and spread over a wider range of sensitivity values. If there is no change between two consecutive

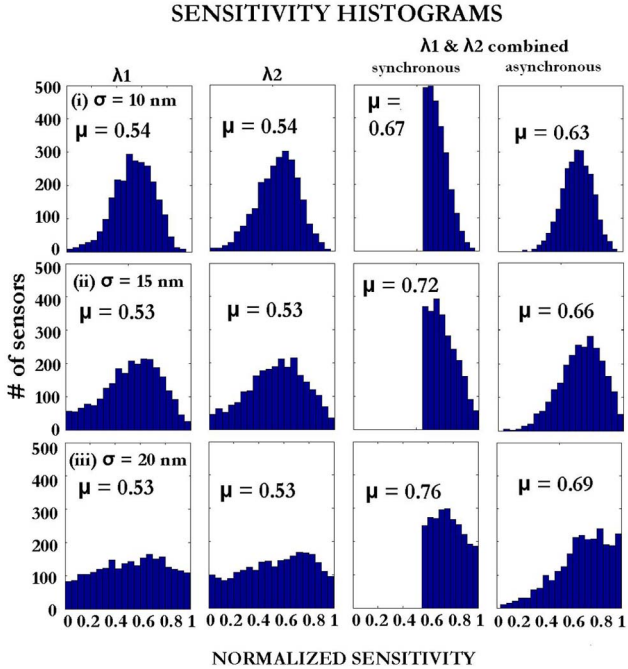

Fig. 3. (Color online) Expected sensitivity histograms with λ_1, λ_2, and combined λ_1, λ_2 readout assuming the same set of gap values for the sensor array $g_1 = g_2 = N(g_0, \sigma)$ (synchronous), and assuming different and independent set of gap values: $g_1 = N(g_0, \sigma)$, $g_2 = N(g_0, \sigma)$ (asynchronous), for the sensor array during λ_1, λ_2 measurements for $\sigma = 10$, 15, and 20 nm. "μ" denotes the average sensitivity of histograms.

frames, then the sensitivity is expected to converge to that of the synchronous case.

4. Experimental Results

Sensitivity enhancement was demonstrated using previously fabricated thermal imaging sensor arrays, which relies on a thermomechanical bending principle. The sensor operation principle is thermomechanical, i.e., the structure bends in response to the target temperature. The mechanical displacement creates an intensity change, which is monitored by observing the first diffracted order with a photodetector or a CCD camera for an array of sensors, as illustrated in Figs. 1(b) and 1(c) [9]. A 160×120 array of thermal imaging sensors with a $50\,\mu$m pitch were uniformly illuminated in one shot with two sources of wavelengths 633 and 650 nm, where the beams are expanded and truncated to minimize spatial variations in the beam profile [Fig. 1(b)]. Therefore, the spatial variations in the diffracted order intensities are rather attributed to the nonuniformity in the sensor gaps. Furthermore, it is worthy to note that the optical readout is not limited to sources having equal intensities. Spatial variations of the laser profiles after beam homogenization can be digitally corrected by acquiring a set of calibration images prior to data acquisition. It is best to limit this variation as it would use up the usable dynamic range. The maximum sensitivity point of th e2 – λ readout, which is at $\lambda_S/8$, is found to be $\sim 3\,\mu$m for the wavelength combination, which is sufficiently close to the mean gap $g_0 = 2.25\,\mu$m. The sensor array was placed in vacuum due to performance requirements, in order to eliminate thermal conduction and convection path through the air [9]. Furthermore, an IR lens was placed at the front side of the sensor array to image the target onto the array. A periodic slab cut within a printed circuit board (PCB) of size 6×6 cm, illustrated in Fig. 1(c) and with more detail in Fig. 4(a), was placed in front of an IR heater as a target to have a clear distinction between hot and cold areas. Note that it is necessary to monitor the diffracted order intensity at two different but sufficiently close gap and intensity values in order to approximate the sensitivity term given in Eq. (3). For a thermomechanical sensor, the change in the gap is linearly proportional with the applied temperature [9]. Therefore, the sensitivity was found based on the intensity change of the sensors with respect to two different heater temperatures: T_1 (heater on) and T_2 (heater off), where $T_1 - T_2 = 250\,^{\circ}$C. In the experimental setup, the data was monitored in real-time with the CCD camera, and saved. Once the procedure was repeated for the second wavelength, the data can be processed within a few seconds using MATLAB computing software.

Figure 4(b) illustrates a zoomed image of the captured first order diffracted light of ~50 sensors. Differential images were calculated for the entire array for both wavelengths, which are illustrated in Figs. 4(c) and 4(d), by subtracting images taken during the on and off states of the heater for two laser sources, in the configuration shown in Figs. 1(b) and 1(c). The sensitivity histograms shown in Figs. 4(f)

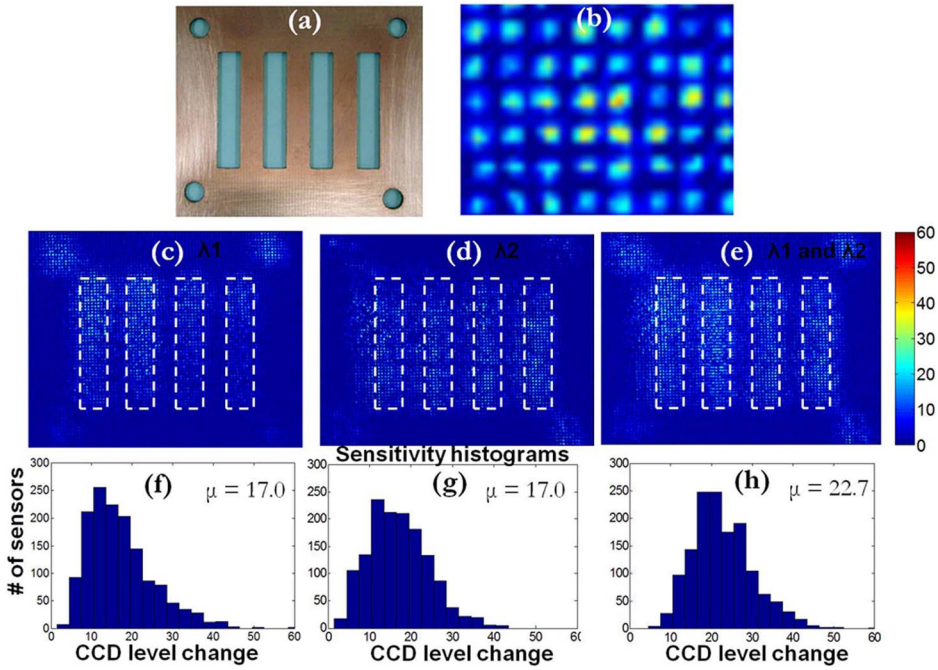

Fig. 4. (Color online) (a) Target used in the experiment: periodic PCB slab, which is placed in front of an IR heater. (b) Zoomed image of about 50 sensors captured by using first order diffracted light. (c) Image of 20, 000 sensors by using first order diffracted light acquired by λ_1. (e) Same image acquired by λ_2. (e) Combined image of (c) and (d) using a postdetection signal processing by taking the larger change with respect to the reference image. (f) Histogram of the λ_1 difference image. (g) Histogram of λ_2 difference image. (h) Histogram of the combined image. The average sensitivity μ increases from 17 CCD levels for each individual image up to 22.7 CCD levels.

Table 1. Comparison of Synchronous and Asynchronous Modes of Operation in Two-Wavelength Readout[a]

Readout Approach	Synchronous Operation	Asynchronous Operation
Sensor gap	$g_1 = g_2$	$g_1 \neq g_2$
Readout camera	2 detector arrays or CCD cameras	1 detector array or a CCD camera[b]
Optical components for wavelength switching	• Polarizing beam splitter	• Pulsing the lasers time-sequentially
	• Narrowband color filters	• Ferroelectric liquid crystals polarization rotator and a polarizer to transmit one laser at a time • Rotating narrowband coated color filters to transmit one laser at a time

[a]A variety of optical hardware components are listed for both modes for wavelength separation.
[b]The asynchronous mode converges to the synchronous case for slowly varying signals.

and 4(g) are displayed based on the absolute intensity changes of the areas shown with white rectangles, which correspond to the openings in the periodic slab, where ~2000 among 20, 000 sensors are illuminated. Finally the combined image [Fig. 4(e)] and histogram [Fig. 4(h)] are calculated based on Eq. (4), where the CCD level changes correspond to $dI(\lambda, g)/dg$ for small CCD level changes observed during the experiment (<40 where full intensity swing is ~150 out of 256 levels).

Sensor-to-sensor gap uniformity variations cannot be directly measured easily. It can be measured using a white light interferometer from the top side; however, this measurement will not account for the layer thickness variations during fabrication. With the proposed method, the gap variation can be estimated using the experimental enhancement in a sensitivity of ~30%. The standard gap deviation of the tested sensor array is then predicted to be $\sigma = 20$ nm, where 30% expected sensitivity enhancement matches the experimental result. The difference between the theoretical and experimental histogram curve shape is attributed to the deviation of the individual sensitivity histograms acquired with both wavelengths separately during the experiment [Figs. 4(f) and 4(g)] from the Gaussian model and the variations within the mechanical response of the sensors to temperature change.

The synchronous mode is preferable and results in higher sensitivity enhancement; however, it ideally requires two cameras, polarizers, or narrowband dichroic beam splitters, which increases the cost and expands the setup space. The synchronous mode can also be achieved using a single camera, as illustrated in Fig. 1, when the signal is not rapidly changing. However, the asynchronous mode of operation becomes essential when the signal is rapidly changing and a single camera is used for the measurement, which will result in different sensor gaps for two consecutive frames. The asynchronous mode is a realistic model that matches better with the experimental conditions in our proof-of-principle experiments, where the λ_1 and λ_2 measurements were taken several seconds apart and without a closed-loop sensor temperature controller. Therefore, one can assume they are statistically independent due to temperature drift. For real-time thermal imaging applications, the time between two measurements will be about 1/60 s, and the variation will be much smaller. Table 1 compares the differences and optical hardware requirements for both modes of operation.

The sensor array that is used in the experiment can image temperature differences on the order of several degrees [9] using 8 bit CCD detection. On the other hand, the proposed architecture is by no means limited to the performance of the sensor under testing. Improved temperature resolution (<0.1 C noise equivalent temperature difference) and high dynamic range can be obtained by tailoring the mechanical design of the sensor and by using a CCD camera with higher dynamic range.

5. Conclusions and Discussion

Using two or multiple sources for optical readout is a suitable technique for diffraction grating based sensor arrays with enhanced sensitivity performance and extended range. Furthermore, it does not require any modifications on the sensor structure with respect to single source readout, and no active connections to the sensors are needed within the array. The proposed two-wavelength readout scheme was implemented on a thermal imaging sensor array of approximately 20, 000 pixels. A 30% increase in average sensitivity is demonstrated and validated by theory.

Real-time thermal imaging videos with the proposed method can be realized by imaging diffracted order(s) of the two sources onto the CCD camera(s) and acquiring the data of one source at a time or simultaneously. The time multiplexing scheme, where only a single camera is required, can be implemented using various methods, such as time-multiplexed and synchronized intensity modulation and the capture of both sources or by placing a rotating optical filter before the CCD plane. Besides the optical hardware requirements listed in Table 1, the integration of the readout electronics card around a low cost complementary metal-oxide-semiconductor/CCD sensor unit is also required in practice for processing the output signal into a video output format using a digital signal image processor [18]. After the calibration procedure, the sensitivity map of the array for both wavelengths can be stored in dedicated memories, which can serve as a guideline in wavelength

selection for individual sensors. The sensitivity map is to be recalculated once every few minutes to compensate significant changes in the signal content.

Besides thermal imaging sensor arrays, this method paves its way for a variety of highly parallelized sensing applications, such as biosensor arrays, grating spectrometers, and atomic force microscopy, for improved measurement range and sensitivity.

HÜ acknowledges the support from TÜBA-GEBİP award, and OF thanks TÜBİTAK for graduate student fellowship.

References

1. G. G. Yaralioglu, S. R. Manalis, A. Atalar, and C. F. Quate, "Analysis and design of an interdigital cantilever as a displacement sensor," J. Appl. Phys. **83**, 7405–7415 (1998).
2. A. G. Onaran, M. Balantekin, W. Lee, W. L. Hughes, B. A. Buchine, R. O. Guldiken, Z. Parlak, C. F. Quate, and F. L. Degertekin, "A new atomic force microscope probe with force sensing integrated readout and active tip," Rev. Sci. Instrum. **77**, 023501 (2006).
3. O. Manzardo, R. Michaely, F. Schadelin, W. Noell, T. Overstolz, N. D. Rooij, and H. P. Hergiz, "Miniature lamellar grating interferometer based on silicon technology," Opt. Lett. **29**, 1437–1439 (2004).
4. C. Ataman, H. Urey, and A. Wolter, "A Fourier transform spectrometer using resonant vertical comb actuators," J. Micromech. Microeng. **16**, 2517–2523 (2006).
5. H. Torun, J. Sutanto, K. K. Sarangapani, P. Joseph, F. L. Degertekin, and C. Zhu, "Micromachined membrane-based active probe for biomolecular mechanics measurement," Nanotech. **18**, 165303 (2007).
6. C. A. Savran, T. P. Burg, J. Fritz, and S. R. Manalis, "Microfabricated mechanical biosensor with inherently differential readout," Appl. Phys. Lett. **83**, 1659–1661 (2003).
7. E. Timurdogan, N. Ozber, S. Nargul, S. Yavuz, M. S. Kilic, I. H. Kavakli, H. Urey, and B. E. Alaca, "Detection of human *K*-opioid antibody using microresonators with integrated optical readout," Biosens. Bioelectron. **26**, 195–201 (2010).
8. Y. Zhao, M. Mao, R. Horowitz, A. Majumdar, J. Varesi, P. Norton, and J. Kitching, "Optomechanical uncooled infrared imaging system: design, microfabrication, and performance," IEEE/ASME J. Microelectromech. Syst. **11**, 136–146 (2002).
9. M. F. Toy, O. Ferhanoglu, H. Torun, and H. Urey, "Uncooled infrared thermomechanical detector array: design, fabrication, and testing," Sens. Actuators A Phys. **156**, 88–94 (2009).
10. B. V. Gorp, A. G. Onaran, and F. L. Degertekin, "Integrated dual grating method for extended range interferometric displacement detection in probe microscopy," Appl. Phys. Lett. **91**, 083101 (2007).
11. O. Karhade, L. Degertekin, and T. Kurfess, "Active control of grating interferometers for extended-range low noise operation," Opt. Lett. **34**, 3044–3046 (2009).
12. C. Polhemus, "Two-wavelength Interferometry," Appl. Opt. **12**, 2071–2074 (1973).
13. F. Bien, M. Camac, H. J. Caulfield, and S. Ezekiel, "Absolute distance measurements by variable wavelength interferometry," Appl. Opt. **20**, 400–402 (1981).
14. O. Ferhanoglu, M. F. Toy, and H. Urey, "Two-wavelength grating interferometry for MEMS sensors," IEEE Photon. Technol. Lett. **19**, 1895–1897 (2007).
15. O. Ferhanoglu and H. Urey, "Sensitivity enhancement of bimaterial MOEMS thermal imaging sensor array using $2-\lambda$ readout," Proc. SPIE **7718**, 77180O (2010).
16. URL: www.hamamatsu.com.
17. P. De Groot and S. Kishner, "Synthetic wavelength stabilization for two-color laser-diode interferometry," Appl. Opt. **30**, 4026–4033 (1991).
18. M. Erdtmann, L. Zhang, G. Jin, S. Radhakrishnan, G. Simelgor, and J. Salerno, "Optical readout photomechanical imager: from design to implementation," Proc. SPIE **7298**, 72980I (2009).